Quantitative mechanistic model reveals key determinants of placental IgG transfer and informs prenatal immunization strategies

Remziye R Erdogan[1], Sepideh Dolatshahi*[1,2]

[1]Department of Biomedical Engineering, University of Virginia School of Medicine, Charlottesville, VA, 22908

[2]Carter Immunology Center, University of Virginia School of Medicine, Charlottesville, VA, 22908

*Corresponding author: E-mail: sd8us@virginia.edu

1

Abstract

Transplacental antibody transfer is crucially important in shaping neonatal immunity. Recently, prenatal maternal immunization has been employed to boost pathogen-specific immunoglobulin G (IgG) transfer to the fetus. Multiple factors have been implicated in antibody transfer, but how these key dynamic regulators work together to elicit the observed selectivity is pertinent to engineering vaccines for mothers to optimally immunize their newborns. Here, we present the first quantitative mechanistic model to uncover the determinants of placental antibody transfer and inform personalized immunization approaches. We identified placental FcγRIIb expressed by endothelial cells as a limiting factor in receptor-mediated transfer, which plays a key role in promoting preferential transport of subclasses IgG1, IgG3, and IgG4, but not IgG2. Integrated computational modeling and *in vitro* experiments reveal that IgG subclass abundance, Fc receptor (FcR) binding affinity, and FcR abundance in syncytiotrophoblasts and endothelial cells contribute to inter-subclass competition and potentially inter- and intra-patient antibody transfer heterogeneity. We developed an *in silico* prenatal vaccine testbed by combining a computational model of maternal vaccination with this placental transfer model using the tetanus, diphtheria, and acellular pertussis (Tdap) vaccine as a case study. Model simulations unveiled precision prenatal immunization opportunities that account for a patient's anticipated gestational length, placental size, and FcR expression by modulating vaccine timing, dosage, and adjuvant. This computational approach provides new perspectives on the dynamics of maternal-fetal antibody transfer in humans and potential avenues to optimize prenatal vaccinations that promote neonatal immunity.

Introduction

Neonates are vulnerable to infections due to their tolerogenic immune phenotype; for the same reason, neonatal vaccinations have been met with limited success to date (1). To provide passive immunity while the neonatal immune system adapts to the environment *ex utero*, maternal immunoglobulin G (IgG) is selectively transferred across the placenta during gestation. Not only do these maternal antibodies confer neonates with passive early life immunity against infectious diseases, but also they shape the trajectory of neonatal immune development by priming the cellular immune response (2–4). Despite this crucial role, the molecular underpinnings of IgG transplacental transport are incompletely described to date.

Though the placenta obstructs maternal-fetal transport of most large molecules, maternal IgG is selectively transported by way of Fc receptor (FcR)-mediated transcytosis. To enter fetal circulation, IgG must undergo transcytosis through two key cellular layers of the placenta: syncytiotrophoblasts (STBs) and endothelial cells (ECs). The neonatal Fc receptor (FcRn) is known to mediate IgG transport through STBs, but whether this mechanism is sufficient for IgG transport through ECs remains unclear (5–7). In addition to FcRn, STBs and ECs express several Fc gamma receptor (FcγR) isoforms with heterogeneous affinity for IgG (8–10). These classical FcγRs may contribute to observed selective placental “sieving” of IgG dependent upon fragment crystallizable (Fc) characteristics, e.g., IgG subclass and N-linked glycosylation (11–14), yet there is conflicting evidence surrounding the involvement of FcγRs in IgG transport (9,10,15,16). Recent studies hypothesized a role for STB-bound FcγRIIIa or EC-bound FcγRIIb in IgG transfer (9,12,17–21), yet others showed FcRn is sufficient for IgG transport in isolated placental ECs *in vitro* and in mouse placenta *in vivo* (14,22,23). Though informative, the experimental methods underlying these findings do not capture the dynamic nature or time scale of placental antibody transport. To disentangle the involvement of non-canonical FcγRs in IgG sieving, innovative methods that recapitulate the longitudinal dynamics of this fundamental process are needed.

Placental antibody transfer can be leveraged by maternal prenatal vaccines which boost pathogen-specific IgG transport to the neonate (24). Identifying improved immunization strategies to maximize neonatal antibody titers is non-trivial. Placental growth and development dynamically regulating IgG transport coupled with known maternal immune adaptations during pregnancy together define a unique immunization design space which poses a challenge to empirical vaccine optimization by clinical trials alone (25). Predictive kinetic-dynamic modeling can be employed to rationally design vaccines that maximize IgG transfer to the neonate. The ability to make *in silico* predictions of vaccine-induced antibody transfer would enable pre-clinical dosing strategy studies, expediting translation of novel therapeutics from bench to bedside.

In the United States, expecting mothers are routinely vaccinated against tetanus, diphtheria, and acellular pertussis (Tdap) during the early third trimester (26), but emerging evidence suggests that this recommendation may not optimally protect the entire population. First, it has been shown that maternal Tdap immunization earlier in gestation results in higher pertussis toxin (PT)- and filamentous hemagglutinin (FHA)-specific IgG in infants regardless of gestational length (26–28). Second, current vaccination efforts are designed to elicit high antibody transfer to term neonates, yet third trimester immunization may not allot sufficient time for the mother to mount a humoral immune response and subsequently transfer antibodies to preterm neonates (28). Collectively, this evidence supports the potential for personalized vaccine approaches that account for factors such as maternal baseline IgG titer, immunization history, placental function, and risk of preterm delivery to maximize pathogen-specific IgG transfer to the neonate, especially among premature neonates.

To uncover the molecular regulators of placental antibody transport and to inform the development of personalized immunization approaches, we developed the first computational model of human placental IgG transfer. In a case study on Tdap immunization, we use this model as an *in silico* testbed for prenatal vaccine design and identify potential strategies to improve transfer of vaccine-induced antibodies, both at a patient-specific and population level. Ultimately, this model-driven investigation sheds light on the dynamic regulation of maternal-fetal IgG transfer

and provides a foundation to develop precision vaccine approaches which promote neonatal immunity.

Results

Mechanistic model recapitulates IgG subclass-specific placental transfer

To elucidate mechanisms of IgG transfer and selective “sieving”, we devised a dynamic model of IgG transplacental transfer. The model consists of ordinary differential equations (ODEs) describing IgG mass transport through the distinct layers comprising the maternal-fetal interface: STB FcRn-mediated transcytosis, diffusion through intervillous stroma, and EC FcRn- and FcγRIIb-mediated transcytosis (Fig 1A) (see Appendix S1 for model equations). FcRn is widely implicated in placental IgG transport; we additionally chose to incorporate FcγRIIb into the model due to its expression in term placental ECs and demonstrated role in EC transcytosis *in vitro* (9,19,29). To account for increasing Fc receptor expression across gestation as observed in human and rat placenta, the total bound and unbound Fc receptors were input to the model as time-varying offline variables (30,31) (Fig S1, Appendix S1). Model parameters were derived from literature when available, and 11 unknown parameters were estimated by fitting predictions of fetal IgG to data obtained from cordocentesis in human pregnancies (Fig 1B, Table 1) (32). Parameter estimation was performed using CaliPro as described elsewhere (32,33) (see Methods). With this optimized parameter set, the model recapitulated dynamics of both bulk and subclass-specific IgG transfer, predicting the IgG subclass transfer hierarchy most frequently reported in literature (IgG1 > IgG3 > IgG4 > IgG2) (Fig 1C, S2 Fig) (11–13,32,34–36).

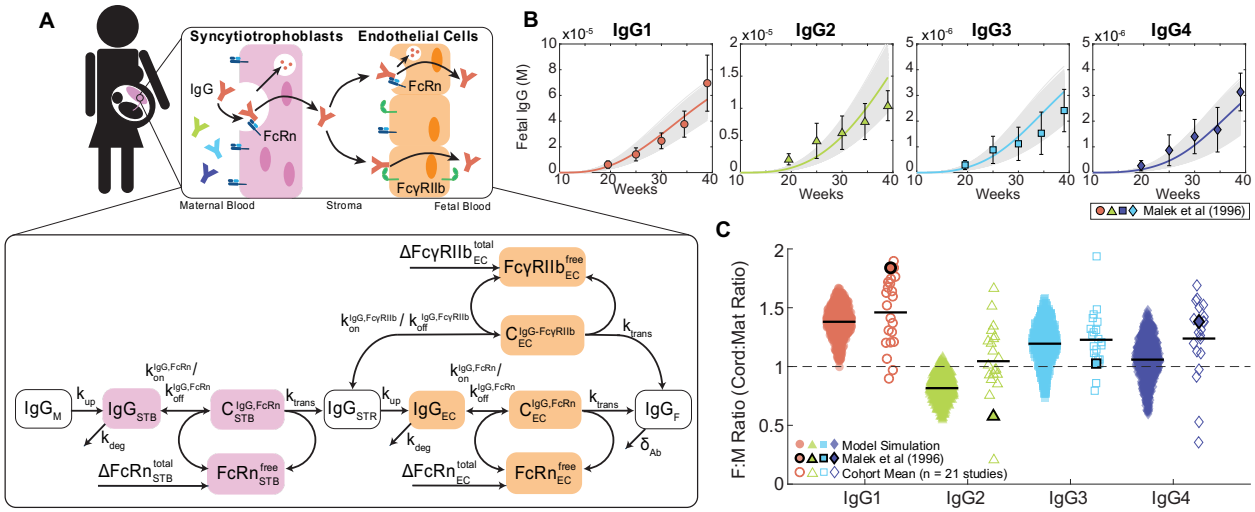

Fig 1. Mechanistic model captures IgG subclass-specific transfer dynamics. (A) The schematic depicts the ODE model representing transport of IgG through the placenta, mapped onto a graphical representation of the maternal-fetal interface. Reaction rate constants associated with each process are depicted on the corresponding arrow. Each box represents a molar concentration in each compartment. "C" denotes complexes of bound IgG and Fc receptors either in endosomes (FcRn) or at the cell surface (FcγRIIb). $\Delta FcRn_{STB}^{total}$, $\Delta Fc\gamma RIIb_{EC}^{total}$, and $\Delta FcRn_{STB}^{total}$ represent synthesis of new FcRn and FcγRIIb molecules over time as the placenta grows. For simplicity, the schematic represents bulk IgG transport, whereas the model includes separate equations for each IgG subclass. (B) Simulated fetal IgG subclass levels vs. time (lines) are overlaid with the data used for parameter estimation. The overlaid data are the mean and standard deviation of IgG subclasses in the umbilical cord between 17-41 weeks gestation (n = 107) measured using cordocentesis by Malek et al (32). Gray lines represent 1000 perturbation simulations resulting from sampling parameters from the ranges determined by CaliPro. (C) The swarm charts show the fetal/maternal ratio (F:M ratio) for each IgG subclass at 40 weeks gestation resulting from 1000 simulations sampling from the optimized range of parameters (filled symbols) compared to the mean cord/maternal ratio for each IgG subclass compiled across cohort studies mined from the literature (hollow symbols). Each symbol represents a single simulation or cohort average. Sample means are indicated by black lines. The symbols outlined in black represent the mean of IgG subclass cord/maternal transfer ratios at parturition from the human study used during parameter optimization (32). Dashed line at F:M ratio = 1 indicates equal concentration in maternal and fetal blood at parturition.

116 **Table 1. List of optimized model parameters.**

Parameter	Value	Units	Interpretation	Source
k_{up}	0.0872-0.0982	L/week	Uptake rate into cells	Optimized
k_{trans}	0.0569-0.0743	L/week	Transcytosis rate	Optimized
k_{deg}	8.4733-9.0809	L/week	Lysosomal degradation rate	Optimized
$FcRn_{STB}^{total,end}$	3.33-4.94e-5	M	STB FcRn expression at term	Optimized
$Fc\gamma RIIb_{EC}^{total,end}$	2.73-3.33e-5	M	EC FcγRIIb expression at term	Optimized
$FcRn_{EC}^{total,end}$	2.36-2.86e-6	M	EC FcRn expression at term	Optimized
$IgG1_0$	3.78e-5	M	Maternal IgG1 concentration	(32)
$IgG2_0$	1.81e-5	M	Maternal IgG2 concentration	(32)
$IgG3_0$	2.35e-6	M	Maternal IgG3 concentration	(32)
$IgG4_0$	2.27e-6	M	Maternal IgG4 concentration	(32)
K_D, FcRn-IgG1 (k_{off}/k_{on})	1.25e-8 (0.15/1.2e7)	M	FcRn and IgG1 dissociation constant	(37,38)
K_D, FcRn-IgG2 (k_{off}/k_{on})	2e-8 (0.15/7.5e6)	M	FcRn and IgG2 dissociation constant	(37,38)
K_D, FcRn-IgG3 (k_{off}/k_{on})	3.3e-8 (0.15/4.5e6)	M	FcRn and IgG3 dissociation constant	(37,38)
K_D, FcRn-IgG4 (k_{off}/k_{on})	5e-8 (0.15/3e6)	M	FcRn and IgG4 dissociation constant	(37,38)
K_D, FcγRIIb-IgG1 (k_{off}/k_{on})	1e-5 (0.15/1.5e4)	M	FcγRIIb and IgG1 dissociation constant	(37,38)
K_D, FcγRIIb-IgG2 (k_{off}/k_{on})	5e-5 (0.15/3e3)	M	FcγRIIb and IgG2 dissociation constant	(37,38)
K_D, FcγRIIb-IgG3 (k_{off}/k_{on})	5e-6 (0.15/3e4)	M	FcγRIIb and IgG3 dissociation constant	(37,38)

K_D, FcγRIIb-IgG4 (k_{off}/k_{on})	5e-6 (0.15/3e4)	M	FcγRIIb and IgG4 dissociation constant	(37,38)
V_M	5.552-5.619	L	Maternal blood volume	Optimized
V_{STB}	0.224-0.258	L	Total STB endosomal volume	Optimized
V_{STR}	0.165-0.179	L	Stromal volume	Optimized
V_{EC}	0.247-0.275	L	Total EC endosomal volume	Optimized
V_F	0.254-0.271	L	Fetal blood volume	Optimized
δ_{Ab}	0.02	L/week	IgG decay rate in the fetus	(39)

Transcytosis rate parameters and Fc receptor expression regulate IgG transfer efficiency and selectivity

To determine the contribution of each parameter to the subclass-specific dynamics predicted by the model, we performed global sensitivity analyses. We generated randomly perturbed parameter sets using Latin Hypercube Sampling (LHS) from uniform distributions spanning the maximum likelihood parameter ranges determined by CaliPro (33,40,41). For each parameter set, the predicted fetal IgG concentration at 40 weeks was calculated. To determine the parameters with the greatest influence on total IgG transfer (Fig 2A-B) and on differential transfer between IgG subclasses defined as entropy of subclasses (Fig 2C-D), orthogonalized partial least squares regression (OPLSR) models were developed using the 1000 perturbed parameter sets to predict either outcome (Methods) (42). Variable importance in projection (VIP) scores revealed that total IgG transfer was most sensitive to the rate of IgG transcytosis by STBs and ECs (k_{trans}), FcRn expressed by STBs, and FcγRIIb expressed by ECs (Fig 2B). On the other hand, all volume parameters negatively correlated with IgG transfer, likely because increasing the volume of either compartment dilutes the IgG concentration. To reveal parameters that contribute to the difference in IgG transfer among IgG subclasses, we built a second OPLSR model predicting the entropy among

IgG subclasses (Methods) (Fig 2C-D). Interestingly, VIP score analysis showed FcγRIIb expressed by ECs and k_{trans} contribute most to the distinct transfer rates among IgG subclasses. FcγRIIb is a low-affinity IgG receptor with highest affinity for subclasses IgG3 and IgG4, suggesting that it constitutes a rate-limiting factor of IgG transfer which fine-tunes the subclass transfer hierarchy (11,15,29). Likewise, k_{trans} acts in an FcR-dependent manner to further amplify the effects of Fc-mediated selectivity. Thus, the rate of cargo internalization and fetoplacental size drives the concentration of bulk IgG in the fetus, whereas FcRn and FcγRIIb collaborate to fine-tune patterns of IgG subclass-specific transfer.

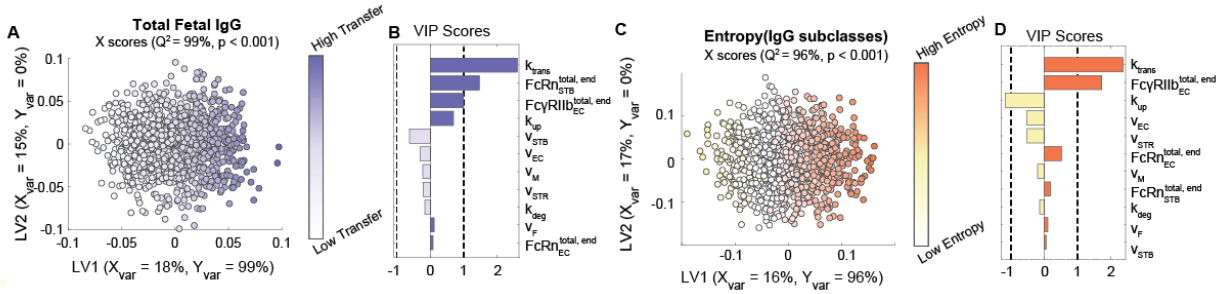

Fig 2. Key parameters associated with transcytosis mechanism and Fc receptor expression regulate IgG transfer. (A-B) An OPLSR model was built to determine parameters predictive of total fetal IgG. (A) The scores plot shows X scores on latent variables 1 and 2 (LV1 and LV2) of simulated fetal IgG concentration at parturition for 1000 randomly perturbed parameter sets. Each circle represents a single perturbation experiment. The points are colored proportional to the resulting simulated concentrations of IgG in the fetus at delivery. The model was orthogonalized such that the direction of maximum variance is in the direction of latent variable 1 (LV1), capturing 99% of the Y variation. The model performed with high predictability power (Q^2 = 99%) and a mean squared error which outperformed 1000 random models with permutated labels ($p < 0.001$). (B) The bar graph depicts the variable importance in projection (VIP) scores, which shows the relative contribution of each parameter to total fetal IgG for a term delivery. VIP scores are artificially oriented in the direction of their loadings on LV1. VIP score > 1 indicates greater-than-average contribution of that parameter. (C-D) An OPLSR model was built to predict entropy among fetal IgG subclass levels at the end of gestation. (C) The scores plot showing X scores on LV1 and LV2 of simulated fetal IgG concentration at parturition for 1000 perturbation parameter sets. Each circle represents a single perturbation experiment. The

points are colored proportional to the resulting simulated concentrations of IgG in the fetus at delivery. The model was orthogonalized such that LV1 captures features associated with the highest entropy, accounting for 96% of the Y variation. The model performed with high predictability power (Q^2 = 96%) and a mean squared error which outperformed 1000 models based on randomly permutated labels ($p < 0.001$). (D) The VIP scores bar plot shows the relative contribution of each parameter to the entropy of IgG subclasses in fetal blood for a term delivery. VIP scores are artificially oriented in the direction of their loadings on LV1.

Endothelial cell-bound FcγRIIb is a key driver of subclass-specific IgG transfer

It is well-established that placental IgG transport increases during the third trimester in humans, so we asked whether increasing FcγRIIb or FcRn expression in ECs drives increased transport efficiency. To gain insight into the expression dynamics of the genes coding for FcγRIIb and FcRn, namely *FCGR2B* and *FCGRT* (FcRn heavy chain), in fetal ECs across gestation, we analyzed two single cell RNA sequencing (scRNA-seq) datasets from published literature spanning three gestational time points: (1) first trimester samples from elective abortions (< 16 weeks), (2) early third trimester samples from preeclamptic cesarean sections (30 weeks), and (3) late third trimester samples from uncomplicated cesarean sections (>37 weeks weeks) (43,44). Interestingly, *FCGR2B* expression was significantly higher in late compared to early third trimester ECs, but we did not detect a significant difference in *FCGRT* expression between early and late third trimester ECs (Fig 3A-B). Conversely, *FCGRT* but not *FCGR2B* transcripts were detected in first trimester ECs, and the ratio of *FCGR2B* to *FCGRT* expression per cell increased across time points (Fig 3C, S3 Fig), suggesting that FcγRIIb dynamically regulates IgG transcytosis in ECs.

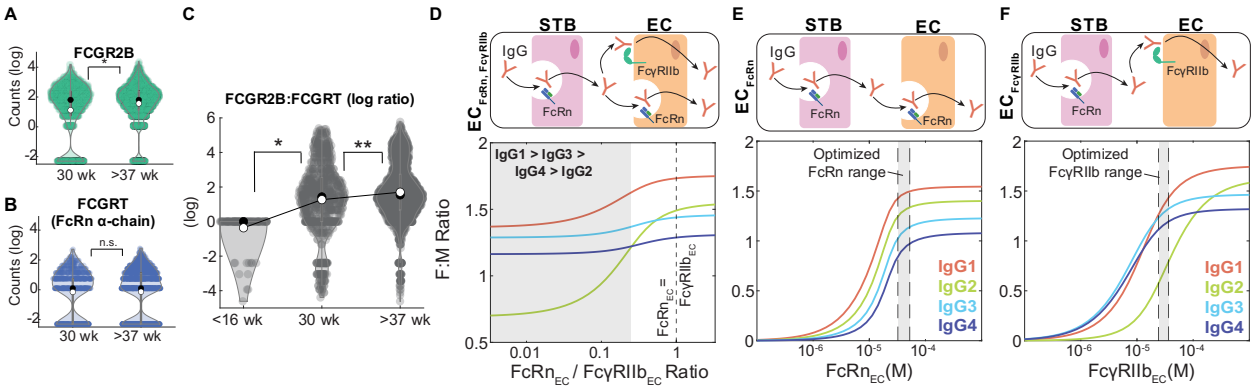

Fig 3. Endothelial cell-bound FcγRIIb is a key driver of subclass-specific IgG transfer. (A-B) Violin plots show *FCGR2B* (A) and *FCGRT* (B) transcript levels in preterm, preeclamptic ECs (30 weeks) compared to term, healthy ECs (>37 weeks) from single cell RNA sequencing data. Black circles represent the sample median, white circles represent the sample mean. (C) Violin plots show the log-transformed ratio of *FCGR2B* to *FCGRT* counts in ECs from single cell RNA seq data from two separate cohorts spanning 3 gestational time points: <16 weeks, 30 weeks, and >37 weeks. Black circles represent the sample median, white circles represent the sample mean. (D-F) Model-simulated IgG subclass transfer ratios as a function of EC Fc receptor expression with ECs expressing FcRn and FcγRIIb (D, $EC_{FcγRIIb\text{-}FcRn}$), only FcRn (E, EC_{FcRn}), or only FcγRIIb (F, $EC_{FcγRIIb}$). The corresponding schematics depict the simulation conditions. Statistical significance in (A-C) was determined by a Wilcoxon rank sum test (* $p < 0.01$, ** $p < 0.001$, n.s. not significant).

Previous studies showed that FcRn and FcγRIIb are co-expressed by placental ECs at the protein level (9,45). Since FcRn has a greater affinity for all IgG subclasses (Table 1), it is unclear whether FcRn alone is responsible for IgG transfer across fetal ECs (22). To assess the contribution of FcγRIIb to IgG transport, we tested whether FcγRIIb is a determinant of subclass-specific transfer. In the model with FcRn and FcγRIIb co-expressed ($EC_{FcRn,FcγRIIb}$), we found that the predicted subclass transfer hierarchy was IgG1 > IgG3 > IgG4 > IgG2 when FcRn expression was less than 25% of FcγRIIb (Fig 3D), demonstrating that higher relative expression of FcγRIIb to FcRn by ECs drives subclass-specific IgG placental transfer. As FcγRIIb binds subclasses IgG1, IgG3, and IgG4 with greater affinity than IgG2, we hypothesized that FcγRIIb is necessary to predict

preferential transfer of IgG1, IgG3, and IgG4 over IgG2. To test this hypothesis, we compared model-predicted fetal-maternal IgG ratios from simulations assuming ECs solely express FcRn (EC_{FcRn}) or FcγRIIb ($EC_{FcγRIIb}$). The EC_{FcRn} model did not capture the preferential transfer of IgG1, IgG3, and IgG4 at any FcRn expression level (Fig 3E). Interestingly, in the $EC_{FcγRIIb}$ model the subclass transfer hierarchy shifted from IgG3 > IgG4 > IgG1 > IgG2 to IgG1 > IgG2 > IgG3 > IgG4 with increasing FcγRIIb expression, indicating FcγRIIb drives the observed subclass transfer hierarchy in humans (Fig 3F). Together, these data implicate FcγRIIb in ECs as a key regulator of antibody transfer dynamics across gestation.

IgG subclasses compete for receptor-mediated transcytosis

Our finding that FcγRIIb limitation plays a key role in determining the subclass transfer hierarchy suggests that maternal IgG subclasses compete for receptor-mediated transcytosis. On the other hand, variation in IgG subclass abundances across individuals may contribute to patient-specific differences in IgG subclass transfer. In agreement with this hypothesis, the placental transport model predicted that all four IgG subclasses transferred less efficiently when mixed compared to each subclass in isolation of the others and the effect of mixing was greater for subclasses with low abundances in maternal serum at low FcγRIIb expression levels (S4 Fig). To further elucidate the role of inter-subclass competition in determining transport efficiency, we explored the effect of IgG1 on IgG4 transcytosis in ECs in a separate model of transcytosis across ECs only (see Methods). We chose to model IgG1 and IgG4 as a case study because they have the highest and lowest abundance in maternal serum, respectively, yet both generally exhibit a cord/maternal ratio > 1 (11,32). Based on a simple kinetic reaction model, the inter-subclass competition can be described by the following closed-form equation:

$$C_{IgG4-FcRn} = \frac{FcRn_0[IgG4]}{K_{D,IgG4}(1 + \frac{[IgG4]}{K_{D,IgG4}} + \frac{[IgG1]}{K_{D,IgG1}})}$$

224 Where $C_{IgG4\text{-}FcRn}$ is the concentration of bound IgG4 and FcRn, $FcRn_0$ is the total concentration of
225 receptor, [IgG1] and [IgG4] are concentrations of maternal IgG1 and IgG4, and $K_{D,IgG1}$ and $K_{D,IgG4}$
226 are their respective equilibrium dissociation constants (see derivation in Methods). Intuitively, $C_{IgG4\text{-}}$
227 $_{FcRn}$ is a function of IgG1 abundance and affinity for FcRn, such that either increasing [IgG1] or
228 decreasing $K_{D,IgG1}$ (i.e., increasing IgG1-FcRn affinity) decreases $C_{IgG4\text{-}FcRn}$ and consequently, IgG4
229 transcytosis.

230 To validate and further characterize competition among IgG subclasses, we used an *in vitro*
231 system to model IgG transcytosis through human umbilical vein endothelial cells (HUVEC) cultured
232 on Transwell permeable membranes (Fig 4A) (Methods). In parallel, we devised a distinct,
233 simplified mechanistic model of receptor-mediated transcytosis in ECs and optimized its parameters
234 by fitting to temporal data of IgG4 transcytosis in the HUVEC experimental system ($[IgG4_{apical}]$ = 0.5
235 or 0.125 mg/ml) (S5 Fig, Table 2). To recapitulate the physiological conditions where FcR is limited,
236 we varied IgG4 levels to determine the concentration of IgG4 where IgG4 transfer no longer
237 increases with increasing apical IgG4 levels. Although HUVEC expresses FcRn but not FcγRIIb,
238 our findings remain valid because the affinities of IgG1 and IgG4 for either receptor are on the same
239 order of magnitude and thus the dynamics of subclass competition are comparable (37). Our
240 mechanistic model predicted that IgG4 transcytosis saturates at $[IgG4_{apical}]$ > 0.33 mg/ml, indicating
241 FcRn limitation; we validated this finding in an analogous *in vitro* experiment in the Transwell
242 system (Fig 4B). To quantify the effect of IgG1 on IgG4 transcytosis, we simulated the effect of
243 increasing IgG1 concentration when IgG4 was fixed at a concentration just below the FcRn
244 saturation point ($[IgG4_{apical}]$ = 0.2 mg/ml). Our model predicted that IgG4 transcytosis would not be
245 affected by the presence of IgG1 until the total IgG concentration exceeded the saturation point—
246 that is, $[IgG1_{apical}] + [IgG4_{apical}]$ > 0.33 mg/ml. In agreement with our computational model prediction,
247 increasing IgG1 caused IgG4 transcytosis to decrease only when the total IgG concentration
248 exceeded the FcRn saturation point (Fig 4C). IgG subclass-specific transfer is thus a function of

249 subclass abundances and FcR affinity, and competition for FcR-mediated transcytosis occurs when

250 FcR expression is limited.

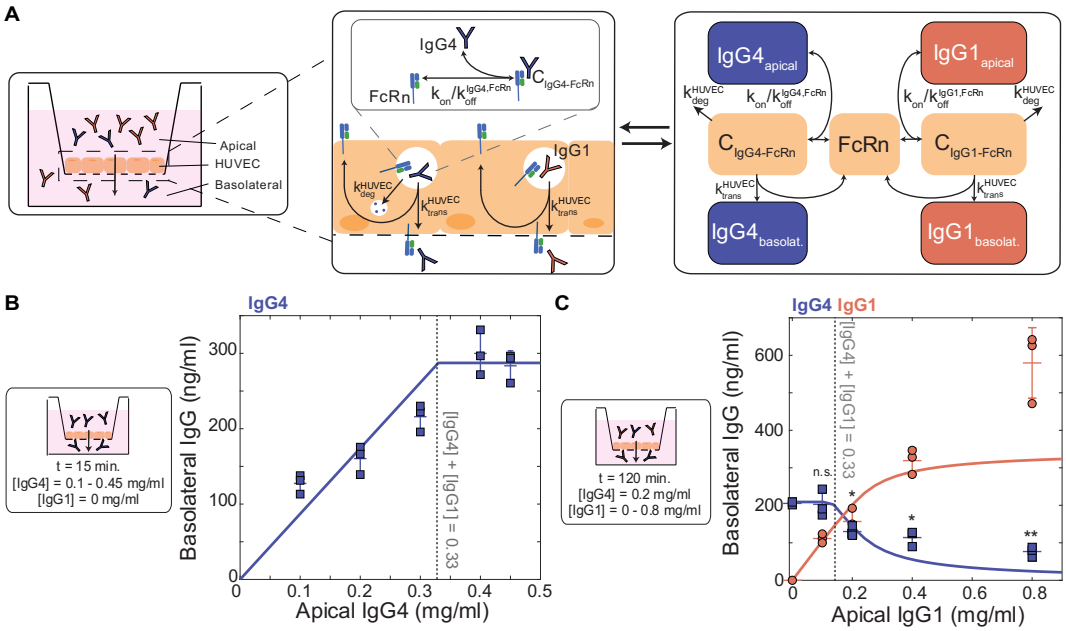

251 **Fig 4. IgG1 competes with IgG4 for FcRn-mediated transcytosis in HUVECs.** (A) Schematic showing a

252 cross-sectional view of the Transwell system and corresponding mechanistic model representation of FcRn-

253 mediated IgG4 and IgG1 transport through HUVEC. Left panel: Arrow indicates the direction of transfer

254 (apical to basolateral). Center panel and right panel: Reaction rate constant associated with each process is

255 depicted on the corresponding arrow. (B) Model-predicted IgG4 transcytosis (y-axis) with increasing apical

256 concentration (x-axis) (solid line) is plotted against experimental data points with the mean and standard

257 deviation from three independent biological replicates. The corresponding experimental conditions are

258 displayed in the panel on the left. The dashed line represents the model-predicted and experimentally

259 validated transcytosis saturation point ($[IgG_{total}]$ = [IgG4] = 0.33 mg/ml). (C) Model-predicted IgG4 and IgG1

260 transcytosis (y-axis) with increasing apical concentration of IgG1 (x-axis) (solid lines) is plotted against

261 experimental data points with the mean and standard deviation from three independent biological replicates.

262 The corresponding experimental conditions are displayed in the panel on the left. The dashed line represents

263 the model-predicted and experimentally validated transcytosis saturation point ($[IgG_{total}]$ = [IgG4] + [IgG1] =

264 0.33 mg/ml. Statistical comparisons shown are between IgG4 in the absence of IgG1 (far left condition) and

265 all combinations of IgG1 and IgG4 mixed using a one-tailed two-sample t-test (* $p < 0.05$, ** $p < 0.001$, n.s.

266 not significant).

267 **Table 2. Optimized HUVEC transcytosis model parameters.**

Parameter	Value	Units	Interpretation	Source
FcRn	2200	nM	HUVEC FcRn expression level	Optimized
k_{deg}^{HUVEC}	0.01	1/minute	Lysosomal degradation rate	Optimized
k_{trans}^{HUVEC}	2.5 x 10^{-5}	1/minute	Transcytosis rate	Optimized
K_D, FcRn-IgG1 (k_{off}/k_{on})	1.25e-8 (0.15/1.2e7)	M	FcRn and IgG1 dissociation constant	(37,38)
K_D, FcRn-IgG4 (k_{off}/k_{on})	5e-8 (0.15/3e6)	M	FcRn and IgG4 dissociation constant	(37,38)

268

269 Optimal Tdap vaccine strategies depend on gestational age, 270 kinetics of the maternal IgG response to Tdap, and Fc receptor 271 expression

272 Considering the new insights into the dynamic regulation of antibody transfer by FcRs revealed by
273 our model, we sought to uncover key features influencing the transfer of vaccine-induced antibodies
274 which could be considered in precision immunization approaches. To this end, we developed an *in*
275 *silico* immunization testbed by layering simulated kinetics of the maternal antibody response post-
276 immunization into the placental antibody transfer model (Fig 5A). As a case study of a maternal
277 vaccine currently in use, we adapted an existing model of plasma cell activation and antibody
278 secretion following malaria infection to recapitulate IgG responses to Tdap immunization in women
279 of child-bearing age (Methods) (Fig 5B, Table 3) (46,47). A dose of antigen representing maternal
280 immunization was applied to the system at three representative gestational ages (t_{vax}) of 10, 20, and
281 30 weeks to stimulate antibody secreting cell proliferation and anti-pertussis toxin IgG (α-PT IgG)
282 secretion and transfer to the fetus (Fig 5C). Interestingly, the interplay of maternal IgG response
283 kinetics and placental transfer results in different IgG transfer dynamics depending on t_{vax}. This non-

intuitive, gestational-age dependent effect on transfer dynamics emphasizes the importance of *in silico* predictions to determine optimal immunization schedules.

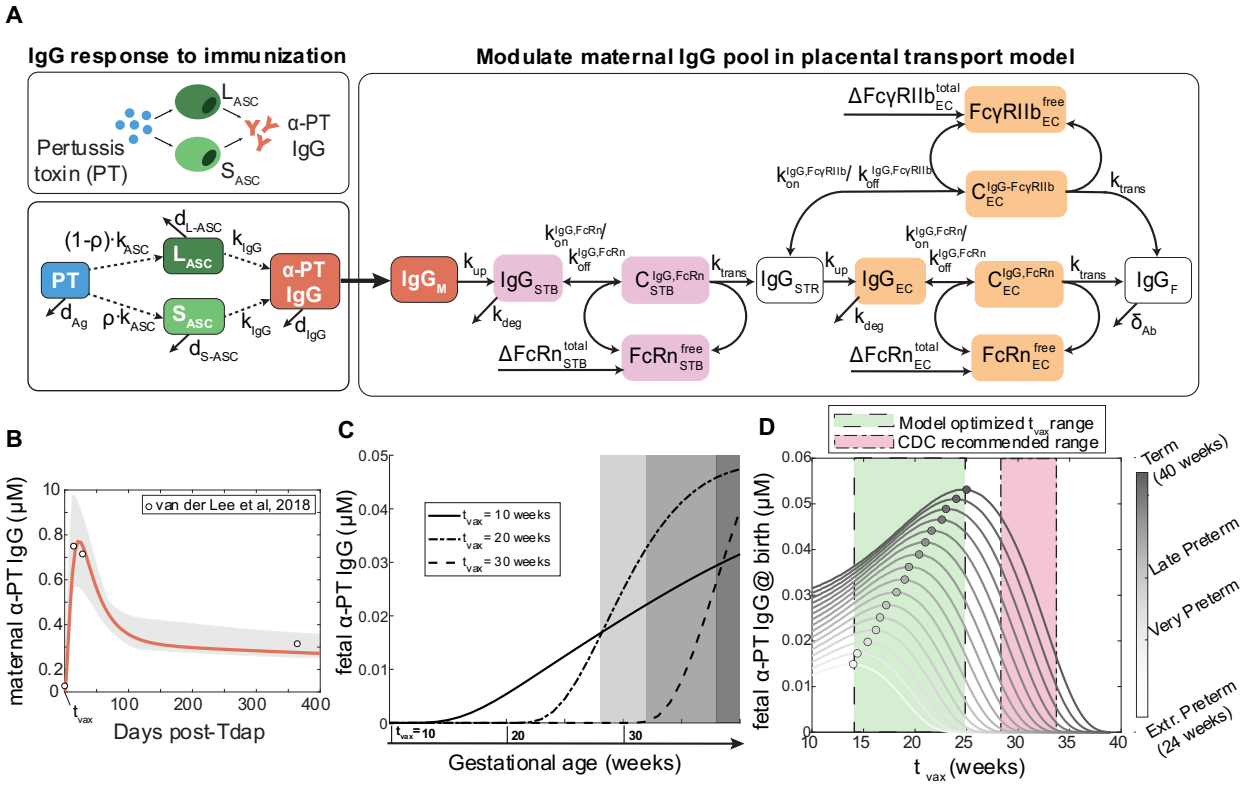

Fig 5. Optimal Tdap immunization time is gestational age dependent. (A) Schematic shows mechanistic model of maternal plasma cell antibody secretion post-vaccination. Vaccine-induced maternal IgG kinetics are integrated into the maternal compartment of the placental IgG transport model, shown in the righthand box. Dashed arrows indicate regulatory processes, solid lines represent processes modeled using mass action kinetics. L_{ASC}: Long-lived antibody secreting cell, S_{ASC}: short-lived antibody-secreting cell, Ag: antigen. (B) Simulated maternal anti-pertussis IgG concentrations vs. time is plotted with a solid line and overlaid with measured IgG concentrations following Tdap vaccination in women of childbearing age from published literature (47) (n = 105). The 95% confidence intervals are shown with light gray shading. (C) Simulated fetal anti-pertussis toxin IgG concentrations are plotted against time following maternal vaccination at three sample vaccination times (indicated along the x-axis): t_{vax} = 10, 20, and 30 weeks gestational age. Shaded regions correspond to gestational length groups (left to right): extremely preterm, very preterm, late preterm, term. (D) Simulated anti-pertussis toxin IgG in the fetus at the time of delivery (y-axis) is plotted over a range of simulated vaccination times (x-axis) and gestational ages (color intensity, color bar on right). The optimal

300 vaccination time and corresponding fetal IgG levels are marked with a circle. The current CDC-recommended
301 maternal vaccination window is highlighted in red, and the model-predicted optimal vaccination range
302 encompassing all gestational age groups is highlighted in green.

303 **Table 3. Pertussis immunization model parameters.**

Parameter	Value	Units	Interpretation	Source
k_{ASC}	0.6	1 / 10^6 PBMCs / day / Ag	Rate of plasma cell generation	Optimized
k_{IgG}	0.0475	mg / ml * (10^6 PBMCs) / days	Rate of antibody production by plasma cells	Optimized
Ag_0	100	mg/ml	Initial dose of antigen	Optimized
ρ	96	%	Proportion of short-lived ASCs (S_{ASC})	(46)
δ_{Ag}	0.15	1 / day	Antigen decay rate	(50)
δ_{IgG}	0.033	1 / day	Antibody decay rate	(46)
$\delta_{S\text{-}ASC}$	0.173	1 / day	Short-lived antibody-secreting cell (S_{ASC}) decay rate	(46)
$\delta_{L\text{-}ASC}$	6.6×10^{-4}	1 / day	Long-lived antibody secreting cell (L_{ASC}) decay rate	(46)

304

305 We next performed simulations over a range of possible immunization times to determine
306 the optimal t_{vax} for newborns born at different weeks of gestation (Fig 5D). Though the correlate of
307 protection for pertussis infection still remains elusive, some possible roles of IgG in pertussis
308 infection include neutralization and opsonophagocytosis (48,49). For the purposes of this study, we
309 assumed that neutralizing antibodies confer protection against pertussis toxin in the neonate and
310 therefore the optimal t_{vax} is defined as the gestational age at immunization resulting in the highest α-
311 PT IgG titer in the fetus at birth. Empirical studies have previously shown that earlier vaccination
312 may be an effective strategy to protect preterm neonates who typically receive a lower quantity of

maternal antibodies (26–28). Using our immunization testbed, we first asked how the optimal Tdap administration schedule varies for the average patient delivering at different gestational time points (i.e., term, late preterm, very preterm, or extremely preterm). In the case of term gestation, the model-predicted optimal t_{vax} was during the 25th week of gestation, but Tdap immunization as early as the 10th week still resulted in greater than half of the optimal IgG concentration being transferred to term newborns (Fig 5D). Optimal t_{vax} scaled with increasing gestational length, suggesting that risk for preterm birth should be considered when determining prenatal immunization schedules (Fig 5D). Interestingly, we found the optimal t_{vax} fell during the second trimester (between 14-25 weeks) regardless of preterm birth status, which is earlier than the window recommended by the Center for Disease Control and Prevention (CDC) (28-34 weeks) and in agreement with studies reporting higher titer of pertussis antibodies in the fetus following maternal vaccination during second trimester as opposed to third trimester (26,28,51). This optimized Tdap vaccination window was unaffected by the magnitude of the maternal α-PT IgG response but did depend on the existence of a transient spike in maternal α-PT IgG driven by the percentage of S_{ASC} (ρ) (Fig S6-7). While α-PT IgG responses following Tdap are generally characterized by a short-lived spike in IgG, variation in the IgG response kinetics for other target antigens should be considered when applying this model to other vaccines. Thus, the optimal Tdap immunization schedule is gestational length-dependent, but a revised vaccination window earlier in gestation could be an effective population-level strategy to ensure coverage for preterm and term newborns alike.

As other sources of inter-patient variability besides gestational length may influence the effectiveness of prenatal vaccination, we sought to identify further opportunities for patient-specific immunization approaches. To determine key variables that should be considered in immunization schedules, we performed a global sensitivity analysis to uncover parameters with the greatest influence on optimal t_{vax}. We optimized t_{vax} in simulations from 1000 perturbed parameter sets, then built an OPLSR model to predict the optimal t_{vax} given each parameter set (Fig 6A, 6B, Methods). Parameters strongly associated with earlier optimal immunization times included $FcRn_{STB}^{total,end}$ and

v_F; $FcRn_{EC}^{total,end}$ and $Fc\gamma RIIb_{EC}^{total,end}$ similarly had negative loadings on latent variable 1 (LV1), as did several other volume parameters. Intuitively, higher compartmental volumes decrease transfer of vaccine-induced antibodies because IgG concentration is diluted in high volume compartments, and thus earlier vaccination enables more IgG to accumulate in the fetus to compensate for this dilution. Likewise, higher $FcRn_{STB}^{total,end}$ facilitates IgG transport into the placental stroma making IgG subsequently available for trans-EC transport. If sufficient $FcRn_{STB}^{total,end}$ is expressed, earlier immunization corresponds to increased levels of IgG accumulated in the stroma, readily available for trans-EC transport. On the other hand, k_{trans} corresponds to later optimal immunization timing because if transcytosis efficiency increases, it confers greater benefit to timing the maternal IgG spike post-vaccination when FcRn and FcγRIIb are expressed in higher quantities. Therefore, differences in fetoplacental size and function across the population may play a role in determining the ideal patient-specific immunization program.

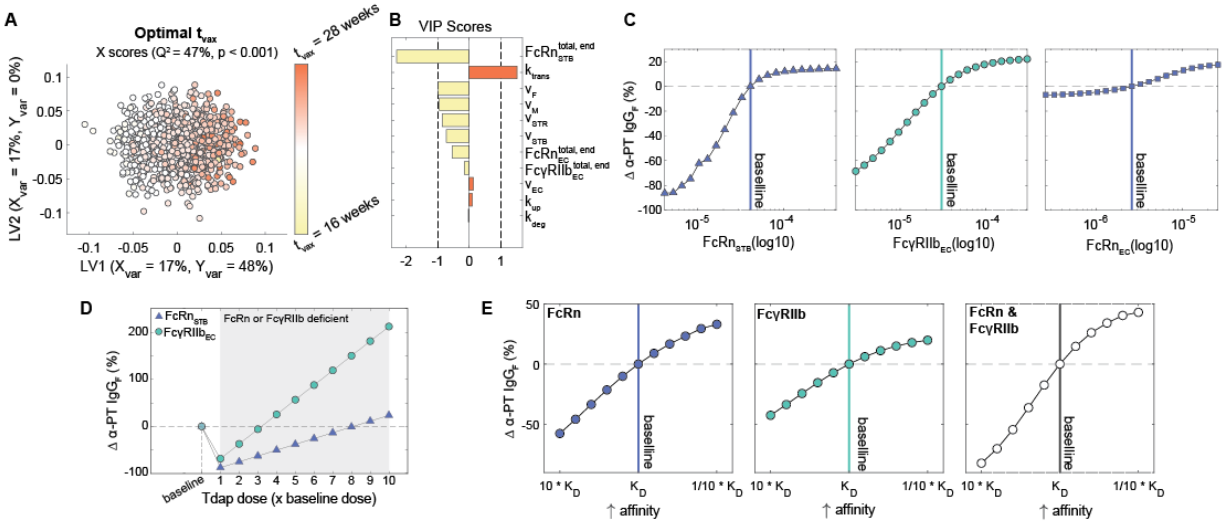

Fig 6. Model reveals opportunities for personalized vaccination strategies. (A-B) The OPLSR model predicts the optimal immunization time (t_{vax}, weeks gestational age) from perturbed parameter sets. (A) The scores plot depicts the X scores on LV1 and LV2 of the optimal t_{vax} for 1000 perturbed parameter sets. Each circle represents a single perturbation experiment colored proportionally to the predicted optimal t_{vax}. The model was orthogonalized such that LV1 is in the direction of maximum variance. (B) The bar plot shows VIP scores that quantify the relative contribution of each parameter to the optimal t_{vax}. VIP scores are artificially

357 oriented in the direction of their loadings on LV1. The model performed with predictive power (Q^2 = 47%) and
358 with a mean squared error lower than 1000 models based on randomly permutated labels ($p < 0.001$). (C)
359 The value of $FcRn_{STB}^{total,end}$ (left), $Fc\gamma RIIb_{EC}^{total,end}$ (center), or $FcRn_{EC}^{total,end}$ (right) was varied from 10-fold lower
360 to 10 times higher than the mean of their optimal range determined by Calipro. Vaccination was simulated at
361 the optimal time for a term newborn (t_{vax} = 25 weeks) for each FcR condition and the resulting percent
362 changes in anti-pertussis toxin IgG (α-PT IgG) in a newborn delivered at 40 weeks is depicted. The dashed
363 line represents the baseline simulation of an average patient using the optimized values of $FcRn_{STB}^{total,end}$,
364 $Fc\gamma RIIb_{EC}^{total,end}$, or $FcRn_{EC}^{total,end}$, which are marked by vertical lines. (D) The chart shows the effect of
365 increasing vaccine dosage on α-PT IgG transfer for patients with a 10-fold deficiency in $FcRn_{STB}^{total,end}$ or
366 $Fc\gamma RIIb_{EC}^{total,end}$ expression. Dosages are shown as fold-changes from the baseline simulation dosage. (E)
367 The effect of increasing vaccine-induced α-PT IgG affinity for FcRn or FcγRIIb on α-PT IgG transferred to a
368 fetus delivered at term.

369

370 With the assumption that maternal IgG protects the fetus via neutralization, the effectiveness
371 of maternal vaccination is ultimately determined by the concentration of maternal antigen-specific
372 IgG in the neonate. Having observed that FcRn and FcγRIIb are key predictors of IgG transport
373 efficiency (Fig 2A), we next investigated the relationship between FcR expression and α-PT IgG
374 transfer efficiency. Consistent with our previous observation that IgG transfer efficiency is highly
375 sensitive to $FcRn_{STB}^{total,end}$ and $Fc\gamma RIIb_{EC}^{total,end}$, we observed a 10-fold decrease in $FcRn_{STB}^{total,end}$ or
376 $Fc\gamma RIIb_{EC}^{total,end}$ diminished α-PT IgG transfer by 86 or 69% respectively, whereas $FcRn_{EC}^{total,end}$ had
377 a minor impact on α-PT IgG in the fetus (Fig 6C). Given that FcR expression is likely variable
378 across the population, we sought to determine vaccination modifications that could potentially
379 compensate for deficiency in either receptor. First, we found that patients with a 10-fold decrease in
380 $FcRn_{STB}^{total,end}$ could transfer comparable levels of α-PT IgG to their fetus by increasing the vaccine
381 dosage 8-fold, and a 10-fold decrease in $Fc\gamma RIIb_{EC}^{total,end}$ could be compensated for by increasing

382 the dosage 3-fold (Fig 6D). Naturally, vaccine dosage can only be increased to the extent that it
383 does not induce toxicity. Rather than increasing the *quantity* of maternal vaccine-induced IgG, we
384 asked whether modulating the *affinity* of vaccine-induced IgG to FcRs (*e.g.* via Fc glycosylation
385 modulation) could improve placental transfer. While precision vaccination is a relatively new
386 concept, recent studies have demonstrated that adjuvants play a key role in driving the glycan
387 profile of vaccine-induced IgG (52,53). Coincidentally, it has been shown that decreasing core
388 fucosylation can improve IgG binding to FcγRIIb and terminal galactosylation increases IgG affinity
389 to FcRn (12,54,55). Our model predicted that decreasing $K_D^{IgG1-4,FcRn}$ by 10-fold increased α-PT
390 IgG transfer by 30%, and a similar relationship was observed for $K_D^{IgG1-4,Fc\gamma RIIb}$ (Fig 6E).
391 Interestingly, the effect of increasing affinity for both receptors was greater than the sum of its parts,
392 suggesting affinity for both receptors can be targeted simultaneously to improve prenatal vaccine
393 efficacy.
394

395 # Discussion

396 Placental antibody transfer is key to protect neonates against infection and to shape the trajectory
397 of early-life immune development (56). Recently, maternal prenatal immunization has been
398 employed to boost antigen-specific antibody transfer to the fetus, providing targeted immunity to the
399 newborn (57). Current prenatal vaccine regimens are applied at the population level, but variation in
400 gestational length, placental size and function, and maternal immune responses present
401 opportunities for patient-specific vaccine approaches. To this end, we developed a computational
402 model to elucidate the features regulating maternal-fetal IgG transport and to inform prenatal
403 immunization strategies. Our modeling approach enabled longitudinal probing of placental antibody
404 transfer dynamics, shedding light on an otherwise black-boxed system. In contrast to prior studies
405 attempting to uncover mechanisms of selective antibody transfer through a variety of *in vitro*, *ex*

406 *vivo*, and *in vivo* approaches, our computational approach recapitulates the dynamics of this
407 process as it occurs in humans (14,21,58,59).

408 Our dynamic model predicted subclass-specific IgG transfer ratios that agree with the trend
409 most commonly reported in the literature: IgG1 > IgG3 > IgG4 > IgG2 (11). While this phenomenon
410 of subclass selectivity has long been recognized, our model provides a mechanistic basis for
411 selective transfer of IgG subclasses based on competition for binding to FcRs that are expressed in
412 limited quantities. Previous studies have demonstrated that competition for FcRn binding
413 contributes to the short half-life of IgG3 (58). Our study builds upon this finding by revealing that
414 FcγRIIb in placental ECs similarly contributes to selective transfer by preferentially binding IgG1,
415 IgG3, and IgG4 with the highest affinity. Moreover, we built a mathematical model that quantifies
416 competition between two IgG subclasses as a function of FcR expression level, maternal IgG
417 subclass abundance, and Fc-FcR interaction affinity. Thus, the subclass transfer hierarchy of IgG1
418 > IgG3 > IgG4 > IgG2 can be explained by each subclass' relative abundance and affinity for FcRn
419 and FcγRIIb. Not only that, but inter-patient variability in subclass abundances, IgG-FcR affinity
420 arising from differential IgG glycosylation, and placental FcR expression can explain discrepancies
421 in this subclass transfer hierarchy across individuals and patient cohorts.

422 Previous studies have identified independent mechanisms of both FcγRIIb- and FcRn-
423 mediated EC transcytosis in placental ECs (29,45), yet the role of FcγRs in placental transport
424 remains highly contested (14,15,60). Our computational framework enabled us to disentangle the
425 contributions of FcRn and FcγRIIb to EC transcytosis, revealing that in an average placenta FcγRIIb
426 drives selectivity of IgG transfer and may play a key role in dynamic regulation of this process
427 across gestation. Together, these observations support the potential role of non-canonical FcγRs
428 driving antibody transfer dynamics and provide a mechanistic basis for previously reported
429 placental IgG "sieving" (12,13,61). Further evidence implicating FcγRIIb in placental transfer include
430 (1) our analysis of scRNA-seq data revealed an increase in *FCGR2B* transcript counts across
431 gestation and (2) placental ECs express the splice variant FcγRIIb2—the isoform capable of

432 endocytosis and expressed by liver sinusoidal endothelial cells, B cells, and macrophages (62–64).
433 In the same vein, previous studies indicate a potential role for FcγRIIIa in STB transcytosis
434 (12,15,35). However, the data supporting FcγRIIIa involvement in placental transfer are purely
435 associative and lack the necessary mechanistic insight to substantiate the inclusion of FcγRIIIa in
436 this model (12,65). To disentangle the roles of FcRn, FcγRIIb, and FcγRIIIa in IgG transcytosis,
437 future studies that uncover the expression patterns and dynamics of these receptors in human
438 placenta and/or experimentally test their effect on IgG transcytosis are warranted.

439 This unique modeling approach allowed us to predict optimized Tdap immunization
440 schedules and identify features affecting optimal Tdap timing during pregnancy, with broad
441 implications for prenatal vaccination both at the population level and as a basis for patient-specific
442 vaccine approaches. First, the model predicted that the optimal Tdap immunization time for an
443 average patient to maximize α-PT IgG transfer is during the second trimester for term and preterm
444 neonates alike, aligning with key findings from other recent studies that Tdap immunization earlier
445 in gestation provides higher α-PT and α-FHA IgG in the newborn (28). While this optimal Tdap
446 administration window was not sensitive to the magnitude of the maternal IgG response, it did
447 depend on the existence of a transient spike in IgG post-vaccination which is not inherent to IgG
448 responses to all antigens. Therefore, these insights may not necessarily be extrapolated to other
449 prenatal immunization programs. However, it is worth noting that our modeling framework is
450 modular, allowing similar optimization routines to be carried out for other prenatal vaccines so long
451 as there is sufficient data to inform simulations of the maternal antigen-specific IgG response
452 kinetics.

453 From a precision medicine standpoint, the model-driven finding that IgG competes for
454 placental transfer contingent upon subclass abundance, FcR expression, and Fc-FcR affinity
455 provides a basis for improving vaccine formulations and dosing strategies to optimize vaccine-
456 induced IgG transfer efficiency. The mathematical model devised in the current study provides a
457 flexible platform to test these novel vaccination strategies given a set of user-defined inputs. Recent

458 studies suggest that modulating vaccine parameters such as the nature of the target antigen,
459 conjugate, number of doses, route of entry, and choice of adjuvant can fine-tune the pool of
460 maternal vaccine-induced antibodies and the anti-infection capabilities of the IgG transferred to the
461 newborn. For example, protein antigens tend to induce an IgG1 or IgG3 response, while
462 polysaccharide antigens tend to induce an IgG2 response (66); more recent studies suggest that
463 the N-glycan profile of vaccine-induced IgG can be modulated by adjuvant, providing a means to
464 fine-tune Fc receptor binding potential (52,53,67,68). Using our model, we discovered the efficacy
465 of maternal vaccines to transfer IgG to the fetus depended strongly on expression of FcRn in STBs
466 and FcγRIIb in ECs. Our model predicted that readily tunable vaccine design choices such as
467 timing of administration, dosage, and adjuvant are potential compensatory mechanisms to improve
468 α-PT IgG transfer in patients with a deficiency in either FcRn in STBs or FcγRIIb in ECs. In order to
469 make such recommendations, further research is needed to identify readily ascertainable
470 biomarkers of placental FcR expression and/or transcytosis efficiency. As a more immediately
471 actionable insight, we further uncovered a sensitivity of optimal immunization timing to volume
472 parameters including maternal, fetal, and placental stromal volumes, which can be estimated by
473 ultrasound imaging or alternative methods. Moreover, our model is able to quantitatively assess the
474 effect of a perturbed maternal pool of antibodies due to various immunodeficiency disorders,
475 autoimmune disorders and other disorders that modify the maternal pool of antibodies and vaccine
476 response (69). As such, we envision this model as a tool to devise precision immunization
477 approaches that account for maternal vaccination history, baseline pool of antibodies, autoimmune
478 disorders or other immunodeficiencies, and risk for preterm delivery or other pregnancy
479 complications to determine the optimal immunization approach per patient.

480 While this model-driven investigation generated many intriguing insights, there are a few
481 limitations to consider. First, the current model relies on the assumption that all IgG is monovalent
482 with a uniform glycan profile. This is an oversimplification as IgG glycosylation undergoes a
483 dynamic shift during pregnancy (70), which can affect Fc receptor-mediated transfer (12,54).

484 Furthermore, in addition to monomeric IgG, IgG can potentially be transferred as antigen-antibody
485 complexes, which is currently understudied and is not incorporated in our current model (16,34).
486 Second, there is a stark lack of data surrounding human placental development and dynamic fetal
487 IgG levels throughout gestation; many model parameters were unavailable in the literature,
488 necessitating *in silico* parameter optimization. Consequently, we assumed several model
489 components to be constant, including maternal, fetal, and placental volumes and maternal IgG
490 levels. In actuality, these features undergo rapid remodeling and growth across gestation and
491 potentially fine-tune antibody transfer dynamics. Future iterations of the model may benefit from
492 more physiologically accurate dynamics of the developing maternal-fetal interface. To facilitate such
493 a model, further investigations detailing the dynamics of placental growth and FcR expression at the
494 protein level are warranted.

495 Despite its limitations, a key strength of our computational approach is the ability to simulate
496 placental transport dynamics which are prohibitively challenging to study *in vivo*. Using tightly
497 integrated modeling and experimental methods, we probed placental transport across scales in time
498 and space, enabling a more holistic view of the system compared to previous studies in the field.
499 Traditionally, placental IgG transport efficiency is benchmarked by a simple ratio of maternal to
500 umbilical cord IgG titer at birth, in part due to its ease of measurement and interpretability. Not only
501 does this metric mask the nuanced impact of the maternal pool of antibodies, but also it
502 insufficiently describes the highly dynamic and cumulative process of antibody transfer and is thus
503 not capable of describing: (1) important concepts such as placental FcR limitation and antibody
504 subclass competition, (2) the interplay between the maternal pool of antibodies and the vaccine-
505 induced maternal antibodies, and (3) the role of the complex placental functions that rapidly evolve
506 throughout gestation, among other reasons. Our mathematical model challenges this metric as a
507 true measure of “efficiency”. With the advent and accessibility of state-of-the-art high-throughput
508 measurements, it is increasingly feasible to probe placental function and define one or more
509 quantitative measures of transfer efficiency that are conditioned on the maternal pool of antibodies

510 and are linked with distinct model parameters that account for placental size, perfusion, and Fc
511 receptor expression.
512 This study represents a major thrust forward in the field of maternal-neonatal immunology
513 and paves the way towards next generation vaccination programs to fine-tune neonatal immunity
514 against a broad range of pathogens. As current vaccination regimens are continually revised and
515 several novel vaccines are currently in clinical trials, now is an opportune time to increase the
516 prevalence of computational systems biology approaches in maternal-fetal medicine to improve
517 outcomes for vulnerable newborns.
518

519 Methods

520 Mechanistic model of placental IgG transport

521 An ordinary differential equation (ODE) model was formulated to simulate mass transport of IgG1,
522 IgG2, IgG3, and IgG4 across the maternal-fetal interface (Appendix S1). A schematic of the model
523 is given in Figure 1A. Fundamental model assumptions are as follows: (i) all processes obey the
524 law of mass action; (ii) IgG binds FcRn within STB endosomes at an acidified pH and FcγRIIb at the
525 EC surface (7,62,71,72); (iii) binding with either receptor initiates transcytosis; (iv) the effects of
526 FcRn-mediated IgG recycling to the apical STB surface are negligible; (v) unbound IgG in STB
527 endosomes undergoes lysosomal degradation; (vi) all blood volumes, IgG subclass concentrations
528 in maternal blood, and IgG-FcR affinities remain constant throughout gestation; (vii) rate
529 parameters (k_{up}, k_{trans}, and k_{deg}) are equal in STB and EC layers and across IgG subclasses; (viii)
530 stromal cells (e.g., Hofbauer cells, fibroblasts) do not interact with IgG or affect its transfer; (ix) the
531 effect of Fab-antigen interactions is neglected such that all IgG is monovalent; (x) FcR expression
532 increases parabolically across gestation informed by FcRn expression trends in rat placenta (31)
533 (see Appendix S1); (xi) STBs exclusively express FcRn and ECs express both FcRn and FcγRIIb;

534 (xii) the effects of Fc or Fab glycosylation on FcR binding are neglected. All model development and
535 corresponding *in silico* experiments were performed in MATLAB R2022a (Mathworks).
536

537 # Parameter determination

538 In total, 17 parameters were derived from literature and 11 were optimized. K_D parameters were
539 ascertained from Bruhns et al, where the authors determined the equilibrium association constants
540 (K_A) experimentally by surface plasmon resonance (SPR) and we determined K_D by the formula K_D
541 $= 1/K_A$ (8,37). We used these K_D values to determine parameters k_{on} and k_{off} for each Fc receptor
542 and IgG subclass pair. The value of k_{off} for IgG1-FcRn was determined experimentally by Suzuki *et*
543 *al* using SPR (38). We assumed k_{off} to be constant for all subclasses based on evidence from other
544 studies comparing multiple subclasses (73–76). We derived the value of k_{on} for each subclass-FcR
545 interaction from the formula $k_{on} = k_{off} / K_D$. The rate of IgG decay in the fetus (δ_{AB}) was derived from
546 the half-life of IgG1 measured in human infants by the formula $\delta_{AB} = \ln(2)/t_{1/2}$ (39). Remaining
547 parameter ranges were determined by calibrating predictions of IgG subclass levels in the fetus to
548 data from Malek *et al*, where the authors quantified IgG subclass concentrations in umbilical cord
549 blood samples by enzyme linked immunosorbent assay (ELISA) (32). Initial conditions (maternal
550 IgG subclass concentrations) were directly ascertained from (32).
551 We performed parameter estimation for 11 parameters using CaliPro, a flexible optimization
552 software implemented in MATLAB and described by Joslyn et al (33). A key strength of CaliPro is
553 its ability to home in on a biologically relevant range of parameters that recapitulate the system
554 dynamics rather than minimizing a simple cost function. Briefly, we implemented CaliPro using Latin
555 Hypercube Sampling (LHS) from a physiologically plausible range of parameter values as
556 determined by benchmarking studies found in the literature. We defined the pass criteria as model
557 simulations within the upper standard deviation of the data set at the first time point, and are within

558 1.5 times the standard deviation at the final time point. Our termination criteria was set to 95% of
559 model runs meeting the pass criteria.
560

561 # Global sensitivity analysis

562 Global sensitivity analysis was performed using LHS to sample the multi-dimensional parameter
563 space followed by an orthogonalized partial least squares regression (OPLSR) framework, as
564 described in (41,42). OPLSR is a multivariate regression technique that predicts a single outcome
565 (Y) from multiple predictors (X) and is especially suited to model systems with multicollinearity
566 among predictors (77). Briefly, numerous random perturbations to all *parameters* of the model were
567 made simultaneously and resulted in individual model runs per random parameter set. We then
568 leveraged OPLSR to build a model for an output of interest (Y) from the matrix of randomly
569 perturbed parameter sets (X). Specifically, to produce the matrix of predictors, 1000 perturbed
570 parameter sets were generated by LHS from a uniform distribution spanning the maximum
571 likelihood range for each parameter previously obtained from CaliPro. The number of parameter
572 sets tested was fixed to the lowest sample size needed to achieve stable sensitivity analysis results.
573 X is therefore a 1000 x 11 matrix (perturbations x parameters) and Y is a 1000 x 1 vector
574 (perturbations x outcome). First, an OPLSR model was constructed using the matrix of 1000
575 permuted parameter sets to predict the total concentration of IgG in the fetus at 40 weeks gestation.
576 A second OPLSR model was constructed in the same manner to predict entropy among IgG
577 subclasses in the fetus at 40 weeks gestation, defined as:

578 $$P_{IgGi} = \frac{IgG_i}{\sum_{i=1}^{4} IgG_i}$$

579 $$E = -\sum_{i=1}^{4} P_{IgGi} \log\left(P_{IgGi}\right)$$

580 Where E is entropy and P_{IgGi} is the proportion of each subclass in the fetal blood. Model
581 orthogonalization was performed such that the direction of maximum variance was aligned with

582 latent variable 1 (LV1) (78). A third OPLSR model was constructed to determine the sensitivity of
583 the optimal t_{vax} to each parameter.
584 OPLSR model significance was determined empirically by comparing its predictive
585 power (Q^2) against randomly permuted models in a 5-fold cross validation scheme, where Q^2 is
586 defined as:

587 $$Q^2 = 1 - \frac{\sum_i (y_i - f'(x_i))^2}{\sum_i (y_i - \bar{y})^2}$$

588 Where x_i are the corresponding randomly perturbed parameter vectors in matrix X, y_i is each
589 individual outcome in vector Y, and $\bar{y}$ is the mean of all observations in Y.
590

591 HUVEC transcytosis assay

592 Antibody preparation

593 Purified human polyclonal IgG1 and IgG4 (Abcam, AB90283, AB183266) were dialyzed in 1x PBS
594 using Slide-A-Lyzer mini dialysis units with a 10K molecular weight cutoff (Invitrogen, 88404) to
595 remove sodium azide. Dialysis units were incubated at 4°C for 2 hours, then dialysis buffer was
596 changed and incubated again at 4°C for 2 hours. Protein was removed from the dialysis unit using a
597 micropipette and quantified using a NanoDrop Microvolume Spectrophotometer (Thermo Fisher).
598

599 Cell culture

600 6.5 mm diameter Transwell inserts (Corning, CLS3422) coated in 1.4% gelatin were seeded with
601 primary human umbilical vein endothelial cells (HUVEC) (Promocell C-12200, kindly provided by
602 Dan Gioeli at UVA) at a density of 1500 cells/mm^2 (50,000 cells/insert). Cells were cultured in
603 complete endothelial cell growth media (Promocell, C-22110) and incubated at 37°C and 5% CO_2.
604 After 24 hours, the cells were washed in sterile PBS and the media was changed.
605

606 ## Transcytosis assay

607 After 48 hours, the cells were washed in sterile PBS and media containing purified human IgG1 and
608 IgG4 was added to the apical chamber. Cells were incubated at 37°C and 5% CO_2 for 120 minutes.
609 IgG1 and IgG4 in the basolateral media were quantified using human ELISA) IgG1 and IgG4
610 quantification kits (Invitrogen, EHIGG1 and BMS2095) according to the manufacturer's protocol. All
611 conditions were run in triplicate and ELISA measurements were run in duplicate. A 5-parameter
612 logistic standard curve was generated for each assay. Absorbance was read at 450 nm with a
613 correction of 590 nm using an Optima microplate reader within 1 hour of completing the assay.
614 Statistical significance was determined with a one-tailed two-sample t-test comparing each sample
615 containing IgG1 and IgG4 to the sample with IgG4 but without IgG1.

616 To confirm monolayer formation, membrane permeability was quantified for each assay by
617 addition of FITC-dextran (4000 MW, Sigma Aldrich 46944) (0.5 mg/ml) to the apical chamber of
618 each insert. FITC-dextran added to inserts without gelatin coating or HUVEC served as a negative
619 control. The basolateral media was sampled after 120 minutes, and fluorescence was read using
620 the Optima microplate reader. Monolayer permeability (%) was defined as:

621 $$Permeability = \frac{[basolat. FITC - dextran]_{HUVEC}}{[basolat. FITC - dextran]_{blank}} \times 100$$

622 Samples with FITC-dextran permeability greater than 3 standard deviations from the mean were
623 excluded based on faulty monolayer formation (S5 Fig).

624

625 # Mechanistic model of HUVEC transcytosis *in vitro*

626 To simulate the dynamics of IgG1 and IgG4 receptor-mediated transcytosis in HUVEC, a kinetic-
627 dynamic model of FcRn-IgG binding and transcytosis in endothelial cells was formulated:

628 $$\frac{dIgG1}{dt} = -k_{on,1}[IgG1][FcRn] + k_{off,1}[C_1] \ (1)$$

629 $$\frac{dIgG4}{dt} = -k_{on,4}[IgG4][FcRn] + k_{off,4}[C_4] \ (2)$$

630 $$\frac{dFcRn}{dt} = -[FcRn]\left(k_{on,1}[IgG1] + k_{on,4}[IgG4]\right) + \left(k_{off,1} + k_{trans}^{HUVEC}\right)[C_1] + \left(k_{off,4} + k_{trans}^{HUVEC}\right)[C_4] \ (3)$$

631 $$\frac{dC_1}{dt} = k_{on,1}[IgG1][FcRn] - \left(k_{off,1} + k_{trans}^{HUVEC}\right)[C_1] \ (4)$$

632 $$\frac{dC_4}{dt} = k_{on,4}[IgG4][FcRn] - \left(k_{off,4} + k_{trans}^{HUVEC}\right)[C_4] \ (5)$$

633 $$\frac{dIgG1_T}{dt} = k_{trans}^{HUVEC}[C_1] \ (6)$$

634 $$\frac{dIgG4_T}{dt} = k_{trans}^{HUVEC}[C_4] \ (7)$$

635 Where [IgG1] and [IgG4] are apical concentrations of IgG1 and IgG4, [FcRn] is the concentration of
636 FcRn expression in HUVEC, $[C_1]$ and $[C_4]$ are the concentration of bound IgG-FcRn complexes,
637 k_{trans}^{HUVEC} is the rate of transcytosis, k_{on} is the forward rate of reaction, and k_{off} is the reverse rate of
638 reaction (Table 2). The model parameters were optimized by fitting to dynamic data of IgG4
639 transcytosis in HUVECs collected at 15, 30, 60, and 120 minutes ($[IgG4_{apical}]$ = 0.5 and 0.125
640 mg/ml) (S5 Fig). To simplify this model and reveal the effect of subclass-subclass competition in Fc
641 receptor-mediated transcytosis, we derived the closed form of equation (5). We assumed that IgG1
642 and IgG4 are present in excess of FcRn, the system is at quasi-steady state such that
643

644 $$\frac{dC_1}{dt} = \frac{dC_4}{dt} = 0 \ (8)$$

645 Where C is the concentration of IgG-FcRn complexes. Under these assumptions, equations (4) and
646 (5) can be rearranged as

647 $$\frac{k_{on,1}[IgG1][FcRn]}{k_{on,1}[IgG1][FcRn]\left(k_{off,1} + k_{trans}^{HUVEC}\right)} = [C_1] \ (9)$$

648 $$\frac{k_{on,4}[IgG4][FcRn]}{k_{on,4}[IgG4][FcRn]\left(k_{off,4} + k_{trans}^{HUVEC}\right)} = [C_4] \ (10)$$

649 The assumption is then made that the total concentration of receptor does not change such that

650 $$[FcRn] = [FcRn_0] - [C_1] - [C_4] \ (11)$$

651 Substituting (11) into (10):

652 $$\frac{k_{on,4}[IgG4]([FcRn_0] - [C_1] - [C_4]\,)}{k_{on,4}[IgG4][FcRn]\left(k_{off,4} + k_{trans}^{HUVEC}\right)} = [C_4] \ (12)$$

653 And (9) into (12):

654 $$\frac{k_{on,4}[IgG4]\left([FcRn_0] - \frac{k_{on,1}[IgG1][FcRn]}{k_{on,1}[IgG1][FcRn]\left(k_{off,1} + k_{trans}^{HUVEC}\right)} - [C_4]\,\right)}{k_{on,4}[IgG4][FcRn]\left(k_{off,4} + k_{trans}^{HUVEC}\right)} = [C_4] \ (13)$$

655 Solving (13) for $[C_4]$ yields the closed-form solution for IgG4-FcRn complex formation (79):

656 $$C_4 \ = \frac{FcRn_0[IgG4]}{K_{D,4}\left(1 + \frac{[IgG4]}{K_{D,4}} + \frac{[IgG1]}{K_{D,1}}\right)} \ (14)$$

657 Which quantifies the effect of competition between two IgG subclasses undergoing transcytosis in

658 the presence of one Fc receptor.

659

660 # Pertussis (Tdap) immunization simulations

661 To simulate maternal Tdap immunization, a model of plasma cell activation and IgG secretion in

662 response to antigen stimulus was adapted from a previous study by White *et al* in the context of

663 malaria (46). The model consisted of 8 parameters, of which 4 were fitted parameters determined

664 by White *et al*, 1 was determined experimentally by Dari *et al*, and 3 were optimized in this study

665 (50). Parameters were tuned to fit previously published dynamic data of the maternal IgG response

666 to Tdap booster vaccination (47) (Table 3). We assumed several parameters which depend on the

667 host environment—namely, systemic cytokine concentrations and availability of FcRn for IgG

668 recycling and half-life extension—do not depend on antigen-specificity and thus are conserved

669 between malaria and pertussis contexts (80,81). Such parameters were preserved from White *et al*

670 and include the proportion of long-lived antibody secreting cells (L_{ASC}) to short-lived antibody

671 secreting cells (S_{ASC}), the lifespan of L_{ASC} and S_{ASC}, and the antibody decay rate (46). On the other

hand, parameters which depend on the plasma cell niche and context of the specific antigenic challenge (e.g., rates of plasma cell proliferation, antibody secretion, and the antigen decay rate) were optimized to fit titers of anti-pertussis toxin IgG (α-PT IgG) in women of childbearing age following a booster Tdap vaccination (47) (Table 3). Other important model assumptions include: (i) IgG has a half-life of 31 days in the fetus; (ii) the dynamics of B cell activation—including antigen presentation by follicular dendritic cells and cytokine secretion by T cells—and the contribution of memory B cells are neglected; (iii) mothers have been previously exposed to pertussis toxin (i.e., this is a booster vaccine); (iv) all mothers have the same dynamic response to immunization; (v) immunization resulted in equal parts IgG1, IgG2, IgG3, and IgG4 with uniform glycosylation profile and immunoglobulin isotype switching was neglected; (vi) L_{ASC}s and S_{ASC}s secrete IgG with identical subclass and glycosylation profile; (vii) the peak antibody titer is between 14 and 28 days post-immunization; (viii) the IgG response to pertussis is the same in pregnant and non-pregnant individuals (82). Maternal immunization was simulated by stimulating the maternal compartment with antigen at a time t_{vax} (given in weeks gestational age) to induce an antibody response, which directly fed into the maternal compartment of the placental IgG transport model. To determine the optimal t_{vax} corresponding to maximum pertussis toxin-specific IgG transfer to the fetus, iterative simulations were performed over a range of t_{vax} spanning 10-38 weeks gestational age. Sensitivity of the optimal t_{vax} was determined by parameter perturbation and subsequent OPLSR model construction, as described above.

Acknowledgements

We thank the members of the Dolatshahi lab, Drs. Donald J. Dudley and Loren D. Erickson for helpful discussion and feedback. We would also like to thank Dr. Daniel Gioeli and Devin Roller for providing cell lines and support with Transwell assays. We would like to acknowledge Drs. Yuk Ming Dennis Lo, Peiyong Jiang, and Xi Hu from the Chinese University of Hong Kong for sharing

their published single cell transcriptomic data of placental tissue. We acknowledge Research Computing at The University of Virginia for providing computational resources and technical support that have contributed to the results reported within this publication. URL: https://rc.virginia.edu. Research reported in this publication was supported by the Jeffress Trust Award in Interdisciplinary Research as well as the National Institute of General Medical Sciences of the National Institutes of Health under Systems & Biomedical Data Science training program (T32-GM145443). The content is solely the responsibility of the authors and does not necessarily represent the official views of the funding agencies and the National Institutes of Health.

Data and code availability

All data files and codes used to run the model can be found at our GitHub: https://github.com/Dolatshahi-Lab/Transplacental-antibody-transfer-model. Model equations and *in vitro* Transwell assay data are available as Supplemental files.

711 # References

712 1. Pichichero ME. Challenges in vaccination of neonates, infants and young children.
713 Vaccine. 2014 Jun 30;32(31):3886–94.
714 2. Olin A, Henckel E, Chen Y, Lakshmikanth T, Pou C, Mikes J, et al. Stereotypic Immune
715 System Development in Newborn Children. Cell [Internet]. 2018;174(5):1277-1292.e14.
716 Available from: https://doi.org/10.1016/j.cell.2018.06.045
717 3. Simister E, Israel EJ, Patel VK, Taylor SF, Marshak-Rothstein A. neonatal mice.
718 acquisition of maternal IgG by fetal and 2-microglobulin-associated Fc receptor for
719 Requirement for a beta. 1995 [cited 2022 Oct 19]; Available from:
720 http://www.jimmunol.org/content/154/12/6246
721 4. Marchant A, Kollmann TR. Understanding the ontogeny of the immune system to
722 promote immune-mediated health for life. Front Immunol. 2015;6(FEB):77.
723 5. Brambell FW. THE TRANSMISSION OF IMMUNITY FROM MOTHER TO YOUNG AND
724 THE CATABOLISM OF IMMUNOGLOBULINS. Lancet. 1966 Nov 19;288(7473):1087–93.
725 6. Wilcox CR, Holder B, Jones CE. Factors affecting the FcRn-mediated transplacental
726 transfer of antibodies and implications for vaccination in pregnancy [Internet]. Vol. 8,
727 Frontiers in Immunology. Frontiers Media S.A.; 2017 [cited 2021 Jan 15]. p. 1. Available
728 from: www.frontiersin.org
729 7. Simister NE. Placental transport of immunoglobulin G. In: Vaccine. Elsevier BV; 2003. p.
730 3365–9.
731 8. Bruhns P, Iannascoli B, England P, Mancardi DA, Fernandez N, Jorieux S, et al.
732 Specificity and affinity of human Fc receptors and their polymorphic variants for human
733 IgG subclasses. 2009 [cited 2021 Mar 16]; Available from:
734 http://ashpublications.org/blood/article-pdf/113/16/3716/1308575/zh801609003716.pdf
735 9. Bright NA, Ockleford CD, Anwar M. Ontogeny and distribution of Fc gamma receptors in

736 the human placenta. Transport or immune surveillance? J Anat [Internet]. 1994 Apr [cited
737 2021 Jun 16];184 (Pt 2(Pt 2):297–308. Available from:
738 http://www.ncbi.nlm.nih.gov/pubmed/8014121
739 10. Kameda T, Koyama M, Matsuzaki N, Taniguchi T, Saji F, Tanizawa O. Localization of
740 three subtypes of Fcγ receptors in human placenta by immunohistochemical analysis.
741 Placenta. 1991 Jan 1;12(1):15–26.
742 11. Clements T, Rice TF, Vamvakas G, Barnett S, Barnes M, Donaldson B, et al. Update on
743 Transplacental Transfer of IgG Subclasses: Impact of Maternal and Fetal Factors. Front
744 Immunol. 2020;11(September):1–17.
745 12. Jennewein MF, Goldfarb I, Dolatshahi S, Cosgrove C, Noelette FJ, Krykbaeva M, et al.
746 Fc Glycan-Mediated Regulation of Placental Antibody Transfer. Cell [Internet].
747 2019;178(1):202-215.e14. Available from: https://doi.org/10.1016/j.cell.2019.05.044
748 13. Dolatshahi S, Butler AL, Pou C, Henckel E, Bernhardsson AK, Gustafsson A, et al.
749 Selective Transfer of Maternal Antibodies in Preterm and Term Children. 2021 Dec 1
750 [cited 2022 Jun 7]; Available from: https://www.researchsquare.com
751 14. Borghi S, Bournazos S, Thulin NK, Li C, Gajewski A, Sherwood RW, et al. FcRn, but not
752 FcγRs, drives maternal-fetal transplacental transport of human IgG antibodies. Proc Natl
753 Acad Sci U S A. 2020;117(23):12943–51.
754 15. Martinez DR, Fouda GG, Peng X, Ackerman ME, Permar SR. Noncanonical placental Fc
755 receptors: What is their role in modulating transplacental transfer of maternal IgG?
756 Sheppard DC, editor. PLOS Pathog [Internet]. 2018 Aug 30 [cited 2021 Mar
757 15];14(8):e1007161. Available from: https://dx.plos.org/10.1371/journal.ppat.1007161
758 16. Simister NE. Human placental Fc receptors and the trapping of immune complexes.
759 Vaccine. 1998;16(14–15):1451–5.
760 17. Daëron M. FC RECEPTOR BIOLOGY. Annu Rev Immunol [Internet]. 1997 [cited 2022
761 Jun 2];15:203–37. Available from: www.annualreviews.org

762 18. Atyeo C, DeRiso EA, Davis C, Bordt EA, De Guzman RM, Shook LL, et al. COVID-19
763 mRNA vaccines drive differential antibody Fc-functional profiles in pregnant, lactating,
764 and nonpregnant women. Sci Transl Med [Internet]. 2021 Oct 27 [cited 2021 Dec
765 6];13(617):8631. Available from:
766 https://www.science.org/doi/abs/10.1126/scitranslmed.abi8631
767 19. Takizawa T, Anderson CL, Robinson JM. A Novel FcγR-Defined, IgG-Containing
768 Organelle in Placental Endothelium. J Immunol [Internet]. 2005 Aug 15 [cited 2021 Apr
769 29];175(4):2331–9. Available from: http://www.jimmunol.org/content/175/4/2331
770 20. Saji F, Samejima Y, Kamiura S, Koyama M. Dynamics of immunoglobulins at the feto–
771 maternal interface. Reviews of Reproduction [Internet]. 1999 [cited 2021 Apr 20];81–9.
772 Available from:
773 http://citeseerx.ist.psu.edu/viewdoc/download?doi=10.1.1.983.3422&rep=rep1&type=pdf
774 21. Rosenberg YJ, Ordonez T, Khanwalkar US, Barnette P, Pandey S, Backes IM, et al.
775 Evidence for the Role of a Second Fc-Binding Receptor in Placental IgG Transfer in
776 Nonhuman Primates. MBio. 2023 Mar 1;14(2):e0034123.
777 22. Antohe F, Rădulescu L, Gafencu A, Ghe V, Simionescu M. Expression of functionally
778 active FcRn and the differentiated bidirectional transport of IgG in human placental
779 endothelial cells. Hum Immunol. 2001 Feb 1;62(2):93–105.
780 23. Kiskova T, Mytsko Y, Schepelmann M, Helmer H, Fuchs R, Miedl H, et al. Expression of
781 the neonatal Fc-receptor in placental-fetal endothelium and in cells of the placental
782 immune system. Placenta. 2019 Mar 1;78:36–43.
783 24. Niewiesk S. Maternal antibodies: Clinical significance, mechanism of interference with
784 immune responses, and possible vaccination strategies. Front Immunol.
785 2014;5(SEP):446.
786 25. Faucette AN, Unger BL, Gonik B, Chen K. Maternal vaccination: moving the science
787 forward. Hum Reprod Update [Internet]. 2015 Jan 1 [cited 2023 Aug 31];21(1):119–35.

788 Available from: https://dx.doi.org/10.1093/humupd/dmu041
789 26. CDC, Ncird. DEPARTMENT OF HEALTH AND HUMAN SERVICES CENTERS FOR
790 DISEASE CONTROL AND PREVENTION Advisory Committee on Immunization
791 Practices (ACIP) Summary Report. 2016 [cited 2022 Apr 6]; Available from:
792 https://wwwdev.cdc.gov/vaccines/acip/meetings/downloads/min-archive/min-2016-10.pdf
793 27. Healy CM, Rench MA, Swaim LS, Smith EOB, Sangi-Haghpeykar H, Mathis MH, et al.
794 Association between Third-Trimester Tdap Immunization and Neonatal Pertussis
795 Antibody Concentration. JAMA - J Am Med Assoc [Internet]. 2018 Oct 9 [cited 2021 Apr
796 9];320(14):1464–70. Available from: https://jamanetwork.com/
797 28. Eberhardt CS, Blanchard-Rohner G, Lemaître B, Boukrid M, Combescure C, Othenin-
798 Girard V, et al. Maternal Immunization Earlier in Pregnancy Maximizes Antibody Transfer
799 and Expected Infant Seropositivity Against Pertussis. Clin Infect Dis [Internet]. 2016 Apr 1
800 [cited 2022 Apr 6];62(7):829–36. Available from:
801 https://academic.oup.com/cid/article/62/7/829/2463039
802 29. Ishikawa T, Takizawa T, Iwaki J, Mishima T, Ui-Tei K, Takeshita T, et al. Fc gamma
803 receptor IIb participates in maternal IgG trafficking of human placental endothelial cells.
804 Int J Mol Med [Internet]. 2015 May 1 [cited 2021 Jul 22];35(5):1273–89. Available from:
805 http://www.spandidos-publications.com/10.3892/ijmm.2015.2141/abstract
806 30. Lozano NA, Lozano A, Marini V, Saranz RJ, Blumberg RS, Baker K, et al. Expression of
807 FcRn receptor in placental tissue and its relationship with IgG levels in term and preterm
808 newborns. Am J Reprod Immunol. 2018;80(3):1–7.
809 31. Wang Y, Jiang X, He J, Diraviyam T, Zhang X. Quantitative Investigation on Correlation
810 Between IgG and FcRn During Gestation and Lactating Periods in Rat. Am J Reprod
811 Immunol. 2016;75(2):81–5.
812 32. Malek A, Sager R, Kuhn P, Nicolaides KH, Schneider H. Evolution of maternofetal
813 transport of immunoglobulins during human pregnancy. Am J Reprod Immunol.

814 1996;36(5):248–55.
815 33. Joslyn LR, Kirschner DE, Linderman JJ. CaliPro: A Calibration Protocol That Utilizes
816 Parameter Density Estimation to Explore Parameter Space and Calibrate Complex
817 Biological Models. Cell Mol Bioeng. 2021 Feb 1;14(1):31–47.
818 34. Palmeira P, Quinello C, Silveira-Lessa AL, Zago CA, Carneiro-Sampaio M. IgG placental
819 transfer in healthy and pathological pregnancies. Vol. 2012, Clinical and Developmental
820 Immunology. 2012.
821 35. Atyeo C, Pullen KM, Bordt EA, Fischinger S, Burke J, Michell A, et al. Compromised
822 SARS-CoV-2-specific placental antibody transfer. Cell [Internet]. 2021 Feb 4 [cited 2021
823 Mar 23];184(3):628-642.e10. Available from: https://doi.org/10.1016/j.cell.2020.12.027
824 36. Dolatshahi S, Butler AL, Siedner MJ, Ngonzi J, Edlow AG, Adong J, et al. Altered
825 Maternal Antibody Profiles in Women With Human Immunodeficiency Virus Drive
826 Changes in Transplacental Antibody Transfer. Clin Infect Dis [Internet]. 2022 Oct 12
827 [cited 2023 Aug 31];75(8):1359–69. Available from: https://dx.doi.org/10.1093/cid/ciac156
828 37. Bruhns P, Jönsson F. Mouse and human FcR effector functions. Immunol Rev.
829 2015;268(1):25–51.
830 38. Suzuki T, Ishii-Watabe A, Tada M, Kobayashi T, Kanayasu-Toyoda T, Kawanishi T, et al.
831 Importance of Neonatal FcR in Regulating the Serum Half-Life of Therapeutic Proteins
832 Containing the Fc Domain of Human IgG1: A Comparative Study of the Affinity of
833 Monoclonal Antibodies and Fc-Fusion Proteins to Human Neonatal FcR. J Immunol
834 [Internet]. 2010 [cited 2023 Aug 29];184:1968–76. Available from:
835 www.jimmunol.org/cgi/doi/10.4049/jimmunol.0903296
836 39. Sarvas H, Sepp I, Kurikka S, Siegberg R, MJi O. Half-Life of the Maternal IgG1 Allotype
837 in Infants. J Clin Immunol. 1993;13(2).
838 40. McKay MD, Beckman RJ, Conover WJ. A comparison of three methods for selecting
839 values of input variables in the analysis of output from a computer code. Technometrics.

840 2000;42(1):55–61.
841 41. Marino S, Hogue IB, Ray CJ, Kirschner DE. A methodology for performing global
842 uncertainty and sensitivity analysis in systems biology. Vol. 254, Journal of Theoretical
843 Biology. Academic Press; 2008. p. 178–96.
844 42. Surve S V., Myers PJ, Clayton SA, Watkins SC, Lazzara MJ, Sorkina A. Localization
845 dynamics of endogenous fluorescently labeled RAF1 in EGF-stimulated cells. Mol Biol
846 Cell [Internet]. 2019 Feb 15 [cited 2023 Apr 5];30(4):506–23. Available from:
847 https://www.molbiolcell.org/doi/10.1091/mbc.E18-08-0512
848 43. Vento-Tormo R, Efremova M, Botting RA, Turco MY, Vento-Tormo M, Meyer KB, et al.
849 Single-cell reconstruction of the early maternal–fetal interface in humans. Nature
850 [Internet]. 2018 Nov 15 [cited 2021 Jan 15];563(7731):347–53. Available from:
851 https://pubmed.ncbi.nlm.nih.gov/30429548/
852 44. Tsang JCH, Vong JSL, Ji L, Poon LCY, Jiang P, Lui KO, et al. Integrative single-cell and
853 cell-free plasma RNA transcriptomics elucidates placental cellular dynamics. Proc Natl
854 Acad Sci U S A [Internet]. 2017 Sep 12 [cited 2021 Mar 29];114(37):E7786–95. Available
855 from: www.pnas.org/cgi/doi/10.1073/pnas.1710470114
856 45. Antohe F, Rădulescu L, Gafencu A, Ghe V, Simionescu M. Expression of functionally
857 active FcRn and the differentiated bidirectional transport of IgG in human placental
858 endothelial cells. Hum Immunol [Internet]. 2001 [cited 2022 Jun 7];62(2):93–105.
859 Available from: https://pubmed.ncbi.nlm.nih.gov/11182218/
860 46. White MT, Griffin JT, Akpogheneta O, Conway DJ, Koram KA, Riley EM, et al. Dynamics
861 of the Antibody Response to Plasmodium falciparum Infection in African Children. J Infect
862 Dis [Internet]. 2014 Oct 1 [cited 2022 Sep 22];210(7):1115–22. Available from:
863 https://academic.oup.com/jid/article/210/7/1115/2908670
864 47. van der Lee S, van Rooijen DM, de Zeeuw-Brouwer ML, Bogaard MJM, van Gageldonk
865 PGM, Marinovic AB, et al. Robust humoral and cellular immune responses to pertussis in

866 adults after a first acellular booster vaccination. Front Immunol. 2018 Apr 4;9(APR):681.
867 48. Knuutila A, Versteegen P, Barkoff AM, van Gageldonk P, Mertsola J, Berbers G, et al.
868 Pertussis toxin neutralizing antibody response after an acellular booster vaccination in
869 Dutch and Finnish participants of different age groups. Emerg Microbes Infect [Internet].
870 2022 [cited 2023 Apr 12];11(1):956–63. Available from:
871 https://www.tandfonline.com/doi/abs/10.1080/22221751.2022.2053364
872 49. Hovingh ES, Kuipers B, Bonačić Marinović AA, Jan Hamstra H, Hijdra D, Mughini Gras L,
873 et al. Detection of opsonizing antibodies directed against a recently circulating Bordetella
874 pertussis strain in paired plasma samples from symptomatic and recovered pertussis
875 patients. Sci Reports 2018 81 [Internet]. 2018 Aug 13 [cited 2023 Apr 13];8(1):1–11.
876 Available from: https://www.nature.com/articles/s41598-018-30558-8
877 50. Dari A, Boulton M, Neyens M, Le Gars M, Valenzuela B, Shukarev G, et al. Quantifying
878 Antibody Persistence After a Single Dose of COVID-19 Vaccine Ad26.COV2.S in
879 Humans Using a Mechanistic Modeling and Simulation Approach. Clin Pharmacol Ther.
880 2022;
881 51. Vilajeliu A, Goncé A, López M, Costa J, Rocamora L, Ríos J, et al. Combined tetanus-
882 diphtheria and pertussis vaccine during pregnancy: transfer of maternal pertussis
883 antibodies to the newborn. Vaccine. 2015 Feb 18;33(8):1056–62.
884 52. Vestrheim AC, Moen A, Egge-Jacobsen W, Reubsaet L, Halvorsen TG, Bratlie DB, et al.
885 A pilot study showing differences in glycosylation patterns of igg subclasses induced by
886 pneumococcal, meningococcal, and two types of influenza vaccines. Immunity, Inflamm
887 Dis. 2014 Aug 1;2(2):76–91.
888 53. Francica JR, Zak DE, Linde C, Siena E, Johnson C, Juraska M, et al. Innate
889 transcriptional effects by adjuvants on the magnitude, quality, and durability of HIV
890 envelope responses in NHPs.
891 54. Subedi GP, Barb AW. The immunoglobulin G1 N-glycan composition affects binding to

892 each low affinity Fc γ receptor. MAbs [Internet]. 2016 Nov 16 [cited 2023 Aug
893 28];8(8):1512–24. Available from:
894 https://www.tandfonline.com/action/journalInformation?journalCode=kmab20
895 55. Cambay F, Forest-Nault C, Dumoulin L, Seguin A, Henry O, Durocher Y, et al.
896 Glycosylation of Fcγ receptors influences their interaction with various IgG1 glycoforms.
897 Mol Immunol. 2020 May 1;121:144–58.
898 56. Brophy-Williams S, Fidanza M, Marchant A, Way SS, Kollmann TR. One vaccine for life:
899 Lessons from immune ontogeny. J Paediatr Child Health [Internet]. 2021 Jun 1 [cited
900 2021 Jun 30];57(6):782–5. Available from:
901 https://onlinelibrary.wiley.com/doi/full/10.1111/jpc.15511
902 57. Marchant A, Sadarangani M, Garand M, Dauby N, Verhasselt V, Pereira L, et al. Maternal
903 immunisation: collaborating with mother nature. Lancet Infect Dis. 2017 Jul 1;17(7):e197–
904 208.
905 58. Stapleton NM, Andersen JT, Stemerding AM, Bjarnarson SP, Verheul RC, Gerritsen J, et
906 al. Competition for FcRn-mediated transport gives rise to short half-life of human IgG3
907 and offers therapeutic potential. Nat Commun 2011 21 [Internet]. 2011 Dec 20 [cited
908 2022 Dec 9];2(1):1–9. Available from: https://www.nature.com/articles/ncomms1608
909 59. Jennewein MF, Abu-Raya B, Jiang Y, Alter G, Marchant A. Transfer of maternal immunity
910 and programming of the newborn immune system.
911 60. Rosenberg YJ, Ordonez T, Khanwalkar US, Barnette P, Pandey S, Backes IM, et al.
912 Evidence for the Role of a Second Fc-Binding Receptor in Placental IgG Transfer in
913 Nonhuman Primates. MBio [Internet]. 2023 Mar 1 [cited 2023 Jun 26];14(2):e0034123.
914 Available from: https://journals.asm.org/journal/mbio
915 61. Martinez DR, Fong Y, Hang Li S, Yang F, Jennewein MF, Weiner JA, et al. Fc
916 Characteristics Mediate Selective Placental Transfer of IgG in HIV-Infected Women. Cell
917 [Internet]. 2019 [cited 2021 Jan 13];178:190-201.e11. Available from:

918 https://doi.org/10.1016/j.cell.2019.05.046
919 62. Mousavi SA, Sporstøl M, Fladeby C, Kjeken R, Barois N, Berg T. Receptor-mediated
920 endocytosis of immune complexes in rat liver sinusoidal endothelial cells is mediated by
921 FcγRIIb2. Hepatology. 2007 Sep;46(3):871–84.
922 63. Mishima T, Kurasawa G, Ishikawa G, Mori M, Kawahigashi Y, Ishikawa T, et al.
923 Endothelial Expression of Fc Gamma Receptor IIb in the Full-term Human Placenta.
924 Placenta. 2007 Feb 1;28(2–3):170–4.
925 64. Daëron M. FC RECEPTOR BIOLOGY [Internet]. Vol. 15, Annu. Rev. Immunol. 1997.
926 Available from: www.annualreviews.org
927 65. Atyeo C, DeRiso EA, Davis C, Bordt EA, De Guzman RM, Shook LL, et al. COVID-19
928 mRNA vaccines drive differential antibody Fc-functional profiles in pregnant, lactating,
929 and nonpregnant women. Sci Transl Med [Internet]. 2021 Oct 27 [cited 2021 Dec
930 7];13(617):8631. Available from:
931 https://www.science.org/doi/abs/10.1126/scitranslmed.abi8631
932 66. Vidarsson G, Dekkers G, Rispens T. IgG subclasses and allotypes: From structure to
933 effector functions. Front Immunol. 2014;5(OCT):520.
934 67. Alter G, Ottenhoff THM, Joosten SA. Antibody glycosylation in inflammation, disease and
935 vaccination. Semin Immunol. 2018 Oct 1;39:102–10.
936 68. Mahan AE, Jennewein MF, Suscovich T, Dionne K, Tedesco J, Chung AW, et al.
937 Antigen-Specific Antibody Glycosylation Is Regulated via Vaccination. PLoS Pathog.
938 2016 Mar 1;12(3).
939 69. Jefferis R, Kumararatne DS. Selective IgG subclass deficiency: quantification and clinical
940 relevance. Clin exp Immunol. 1990;81:357–67.
941 70. Einarsdottir HK, Selman MHJ, Kapur R, Scherjon S, Koeleman CAM, Deelder AM, et al.
942 Comparison of the Fc glycosylation of fetal and maternal immunoglobulin G. Glycoconj J
943 [Internet]. 2013 Feb 10 [cited 2021 Jan 15];30(2):147–57. Available from: www.ms-

944 utils.org/Xtractor2D.
945 71. Simister NE, Rees AR. Isolation and characterization of an Fc receptor from neonatal rat
946 small intestine. Eur J Immunol [Internet]. 1985 Jan 1 [cited 2022 Nov 21];15(7):733–8.
947 Available from: https://onlinelibrary.wiley.com/doi/full/10.1002/eji.1830150718
948 72. Hunziker W, Mellman I. Expression of Macrophage-Lymphocyte Fc Receptors in Madin-
949 Darby Canine Kidney Cells: Polarity and Transcytosis Differ for Isoforms with or without
950 Coated Pit Localization Domains. [cited 2023 Aug 31]; Available from:
951 http://rupress.org/jcb/article-pdf/109/6/3291/1466358/3291.pdf
952 73. Zinkhan S, Thoms F, Augusto G, Vogel M, Bachmann MF. On the role of allergen-
953 specific IgG subclasses for blocking human basophil activation. Front Immunol. 2022 Oct
954 6;13:892631.
955 74. Derebe MG, Nanjunda RK, Gilliland GL, Lacy ER, Chiu ML. Human IgG subclass cross-
956 species reactivity to mouse and cynomolgus monkey Fcγ receptors. 2018 [cited 2023
957 Aug 29]; Available from: https://doi.org/10.1016/j.imlet.2018.02.006
958 75. Szikora B, Hiripi L, Bender B, Kacskovics I, Iliás A. Characterization of the interactions of
959 rabbit neonatal Fc receptor (FcRn) with rabbit and human IgG isotypes. PLoS One
960 [Internet]. 2017 Sep 1 [cited 2023 Aug 29];12(9):e0185662. Available from:
961 https://journals.plos.org/plosone/article?id=10.1371/journal.pone.0185662
962 76. Datta-Mannan A, Witcher DR, Tang Y, Watkins J, Wroblewski VJ. Monoclonal Antibody
963 Clearance IMPACT OF MODULATING THE INTERACTION OF IgG WITH THE
964 NEONATAL Fc RECEPTOR *. 2007;
965 77. Wold S, Sjostrom M, Eriksson L, Sweden˚˚ S. PLS-regression: a basic tool of
966 chemometrics [Internet]. Vol. 58, Chemometrics and Intelligent Laboratory Systems.
967 [cited 2021 May 20]. Available from: www.elsevier.comrlocaterchemometrics
968 78. Trygg J, Wold S. Orthogonal projections to latent structures (O-PLS). J Chemom.
969 2002;16(3):119–28.

970 79. Salahudeen MS, Nishtala PS. An overview of pharmacodynamic modelling, ligand-
971 binding approach and its application in clinical practice. Vol. 25, Saudi Pharmaceutical
972 Journal. Elsevier B.V.; 2017. p. 165–75.
973 80. Wilmore JR, Allman D. Here, There, and Anywhere? Arguments for and against the
974 Physical Plasma Cell Survival Niche. J Immunol [Internet]. 2017 Aug 1 [cited 2023 Apr
975 12];199(3):839–45. Available from:
976 https://journals.aai.org/jimmunol/article/199/3/839/106408/Here-There-and-Anywhere-
977 Arguments-for-and-against
978 81. Cyster JG, Allen CDC. B Cell Responses: Cell Interaction Dynamics and Decisions. Cell.
979 2019 Apr 18;177(3):524–40.
980 82. Huygen K, Caboré RN, Maertens K, Van Damme P, Leuridan E. Humoral and cell
981 mediated immune responses to a pertussis containing vaccine in pregnant and
982 nonpregnant women. Vaccine. 2015 Aug 7;33(33):4117–23.

983

984

985